Electronic properties of atomically coherent square PbSe nanocrystal superlattice resolved by Scanning Tunneling Spectroscopy

Pierre Capiod, Maaike van Der Sluijs, Jeroen de Boer, Christophe Delerue, Ingmar Swart, Daniel Vanmaekelbergh

Electronic properties of atomically coherent square PbSe nanocrystal superlattice resolved by Scanning Tunneling Spectroscopy

Pierre Capiod

Debye Institute for Nanomaterials Science, Utrecht University, PO Box 80 000, 3508 TA Utrecht, the Netherlands

Maaike van der Sluijs

Debye Institute for Nanomaterials Science, Utrecht University, PO Box 80 000, 3508 TA Utrecht, the Netherlands

Jeroen de Boer

Debye Institute for Nanomaterials Science, Utrecht University, PO Box 80 000, 3508 TA Utrecht, the Netherlands

Christophe Delerue

Univ. Lille, CNRS, Centrale Lille, Univ. Polytechnique Hauts-de-France, Junia, UMR 8520 - IEMN, F-59000 Lille, France

Ingmar Swart

Debye Institute for Nanomaterials Science, Utrecht University, PO Box 80 000, 3508 TA Utrecht, the Netherlands

Daniel Vanmaekelbergh

Debye Institute for Nanomaterials Science, Utrecht University, PO Box 80 000, 3508 TA Utrecht, the Netherlands

E-mail: `d.vanmaekelbergh@uu.nl`

October 2020

Abstract. Rock-salt lead selenide nanocrystals can be used as building blocks for large scale square superlattices via two-dimensional assembly of nanocrystals at a liquid-air interface followed by oriented attachment. Here we report Scanning Tunneling Spectroscopy (STS) measurements of the local density of states of an atomically coherent superlattice with square geometry made from PbSe nanocrystals. Controlled annealing of the sample permits the imaging of a clean structure and to reproducibly probe the band gap and the valence hole and conduction electron states. The measured band gap and peak positions are compared to the results of optical spectroscopy and atomistic tight-binding calculations of the square superlattice band

structure. In spite of the crystalline connections between nanocrystals that induce significant electronic couplings, the electronic structure of the superlattices remains very strongly influenced by the effects of disorder and variability.

Introduction

Two-dimensional semiconductors, often called semiconductor quantum wells, are key materials in opto-electronics. Moreover, electron (hole) gasses confined to two dimensions have been extensively investigated, which led to landmark discoveries such as the quantum Hall[1] and quantum spin Hall effect[2, 3]. It has been shown recently that an extra nanoscale periodicity in the plane can have a major impact on the band structure of the semiconductor[4, 5, 6]. The band gap of the semiconductor remains quasi unaltered, while the shape of the valence and conduction bands is determined by the geometry. A prominent example is the honeycomb nanoscale geometry; theory on several levels has shown that the highest valence and lowest conduction bands feature Dirac cones[6]. This offers the possibility of massless electron (hole) excitations in a genuine semiconductor. Other examples of a nanoscale geometry are the square and the Lieb geometry, which also have a lattice-specific band structure. These band structures have recently been confirmed in artificial lattices based on the electron gas present on a Cu(111)[7, 8, 9] surface, and by coupling vacancy states using a chlorine monolayer on Cu(100)[10].

The fabrication of two-dimensional semiconductor materials with a specific nanoscale geometry is still in its infancy. Lithography and etching techniques have been used to craft a honeycomb geometry in GaAs and InGaAs surfaces[11, 12, 13, 14]. Due to the large unit cell, the bandwidth and electronic dispersion in these systems is still limited (up to 7 meV for a lattice with a period of 36 nm)[14]. In a bottom-up attempt, PbSe semiconductor nanocrystals were used as building blocks to prepare two-dimensional nanostructured semiconductors[15]. PbSe nanocrystals are absorbed at an interface, become crystallographically aligned, and finally attach in an epitaxial way to form atomically coherent two-dimensional systems. Self-assembly and oriented attachment with the formation of crystallographic necks between the nanocrystals resulted in lattices with a square array of nanocrystals (and voids) or a hexagonal array of voids, i.e. a honeycomb geometry. In coherently attached superlattices, the overlap strength and directions of wavefunctions between nanocrystals in a square or honeycomb geometry should be much larger than for nanocrystal arrays in which the nanocrystals are still separated by capping molecules. In the latter, no crystalline necks are formed and the quantum mechanical coupling arise from the interlacing of the ligands at the surface of nanocrystals[16, 17]. This approach allows the engineering of material band structures by controlling the constituent elements of nanocrystals and the structural parameters (nanocrystal sizes, neck sizes, nanogeometries) of the arrays. These tunable parameters open a completely new class of material to explore. However,

these systems still suffer from inhomogeneities in the nanocrystal building block size and in the coupling between the nanocrystals (neck sizes, misorientation between two adjacent nanocrystals creating faulty interfaces), partially clouding the lattice-specific electronic band structure[18, 19, 20, 21, 22, 23, 24, 25, 26]. These inhomogeneities rise questions on electronic couplings and dispersions, and on surface potential fluctuations that need to be understood on simple model systems in order to probe the band structure on more complex systems such as the honeycomb nanogeometry where Dirac cones and flat bands have been predicted[6].

Here, we investigate the band structure of a PbSe superlattice with square geometry, and epitaxial neckings between the nanocrystals using scanning tunneling microscopy and spectroscopy. This method is well-suited for the investigation of disordered systems as the local geometry and the local electronic density of states can be obtained[27]. We compare the band gap, valence hole and conduction electron states with the results of atomistic calculations. Our results indicate a moderate coupling between the nanocrystal sites of the lattice, despite the nanocrystals being epitaxially connected. We conjecture that significant potential barriers are still present between the nanocrystals due to inhomogeneities in the connections. We place our findings in the framework of electronic transport studies that have been reported on these lattices[19, 20, 28]. Finally we make suggestions to improve the electronic coupling and lower the disorder.

Experimental

The synthesis of PbSe nanocrystals (NCs) is adapted from a well established procedure in the literature[18, 29, 30, 31]. For the formation of the square superlattice, we used PbSe nanocrystals as building blocks as their synthesis offers the best control in nanocrystal sizes and results in reproducible and controlled long-range oriented attachment. Moreover, the effective electron mass of the PbSe conduction band structure is small, promising a good quantum mechanical coupling between the nanocrystal envelope functions in the superlattice. The nanocrystals which are dispersed in a non-polar solvent (toluene) are drop-casted on top of a liquid substrate (ethylene glycol). As described in the literature[32, 33, 34], the PbSe nanocrystals self-assemble into a 2D square array with the <100> axis pointing upward (perpendicular to the air-liquid interface), and finally attach via <100>/<100> facet-to-facet connection upon evaporation of the toluene solvent. With our sample, the evaporation was done at 22°C for 1.5 hours, then the liquid substrate was heated to 38°C for 20 minutes to strengthen the necks between the nanocrystals. After formation of the 2D structure, the superlattice is transferred to a Highly Ordered Pyrolytic Graphite (HOPG) substrate. This is done by approaching the substrate parallel to the liquid substrate until a meniscus is formed between the two. Then, the PbSe super-structure is washed with chloroform and immersed in a solution of saturated cadmium iodide in methanol for a (partial) ligand exchange procedure. Iodide and oleate create a hybrid ligand shell which provides

an excellent protection from oxidation[35]. Further washing with methanol removes the exchanged ligands from the superstructure surface. After these procedures, the sample was transferred to the vacuum chamber of a Scanning Tunneling Microscope (STM) for cryogenic microscopy and spectroscopy (see below).

In parallel to the preparation of a STM sample, a part of the same superlattice is characterized by Transmission Electron Microscopy (TEM), see figure 1(a). The TEM image shows a seemingly regular square lattice, with a periodic array of voids. The nanocrystal size-distribution extracted from TEM images shows a reversed log-normal distribution (figure 1(b)). The peak of the size distribution is centered around a diameter of $D = 5.84$ nm. Fast Fourier transform of the TEM shows a center-to-center distance of 6.40 nm $\pm$ 0.20 nm (top-right inset of figure 1(a)), the difference is due to formation of elongated necks in the <100>-type directions. This result is consistent with the observations of Geuchies *et al.*[34]. A careful inspection of the TEM images reveals that the necking varies from nanocrystal to nanocrystal. In the bottom-right inset of figure 1(a), the necking can range from very pronounced (for nanocrystals marked with green dots) with a large d/D ratio (d being the diameter of the neck, D the diameter of the nanocrystal) to non-existent (for nanocrystals marked with red dots), consistent with the literature[19, 28, 32]. On the vast majority of the nanocrystals, the ratio d/D to the neighboring nanocrystals is not homogeneous. This non-homogeneity in the crystalline bridges and nanocrystal sizes is reflected in the band structure (see below for details).

Superlattices prepared by wet chemistry methods form a challenge for cryogenic scanning tunneling microscopy and spectroscopy[27]. The presence of ligands and solvent molecules on the superlattice can impede scanning tunneling microscopy and spectroscopy. Therefore, it is crucial to properly prepare the sample before scanning tunneling experiments. We introduced the prepared samples (see above) into the preparation chamber of a LT-STM (Scienta Omicron) and annealed to a temperature of 140°C for 24 hours in order to remove the excess of ligands, molecules and water at the surface of the 2D structure. The sample is then placed in the LT-STM head where it is cooled down to 4 K for microscopy and spectroscopy. A STM image of the square lattice is presented in figure 1(c). It should be remarked here that stripy artifacts due to ligands are not observed, similar to the results from Ueda *et al.* after *in-vacuo* passivation of a PbSe quantum dot solid with trimethylaluminum vapor[20]. We conclude that the hybrid inorganic/organic shell on our PbSe superlattice, created by the procedure described above, provides a clean and stable tunneling junction. However, in certain regions of the sample, blurry lines can still be seen (see S.I.), which implies that some ligands are loosely bound to the NC surface and can interact with the scanning tip. By scanning at a sufficiently low set-point current, it was possible to image the sample with only minor disturbances coming from the ligands. On the local scale, disorder in the lattice is visible. The added 3rd dimension of the STM image reveals height differences (from 1 to 2 nm) on the sample surface which cannot be seen in the TEM image. These height differences together with irregularities in the in-plane

directions indicate the degree of structural disorder in the superlattice. We assign these imperfections to the size distribution of the building blocks and inhomogeneities in the epitaxial connections of the nanocrystals occurring in the two (001) directions of the rock-salt crystal structure[18, 22, 36].

The tunneling spectra, presented in figure 2(a), were acquired at constant height by placing the tip above a single NC site. A PtIr tip has been prepared by indentations into a copper surface prior to inserting the NC sample[37, 38]. The feedback loop is disconnected while a variable voltage is applied to the tunneling junction. The tunneling current I and conductance dI/dV are measured simultaneously. The differential conductance is obtained with a lock-in amplifier (rms modulation of 10 mV at 271 hz). All spectra were averaged using at least 20 dI/dV sets of reproducible curves. Five spectra (taken on ten different NCs, are displayed in figure 2(a). Additional spectra taken on a second sample, showing the same electronic features, are shown in S.I. The raw zero-conductivity gap is determined to be 0.78 eV $\pm$ 0.03 eV by measuring the energetic spacing of the two broad tunneling resonances visible on both sides of the zero-conductance gap.

In order to accurately estimate the value of the band gap and positions of the peaks, we need to take into account the polarization energies and the lever arm[39, 40]. The polarization energy is the energy needed to put an additional charge in the valence and conduction bands, determined by the difference of dielectric constant of the superstructure and its surrounding. In the case of isolated PbSe nanocrystals of 5.80 nm with a dielectric constant $\epsilon_{NC} = 227$, covered by ligands of a dielectric constant $\epsilon_{out} = 3$, deposited on a metallic surface, the polarization energies can be estimated to be around 70 meV[40]. Since the NCs are in a superlattice on a conductive surface, the dielectric mismatch is far less important than for isolated nanocrystals due to the presence of four neighboring nanocrystals of high dielectric constant and the metallic screening. Hence, the polarization energy can be neglected for the present case (value around 1 meV). The lever arm η corresponds to the ratio of the voltage drop in the tip-nanocrystal junction over the entire voltage drop in the tip-nanocrystal-substrate junction. Typical values are 0.8 for isolated PbSe nanocrystal of 6 nm[27] and 0.85 for an assembly of 5.30 and 7.30 nm PbSe NCs[16]. We therefore set the lever arm to 0.85. This means that the single particle band gap of the superstructure, derived from STS, is 0.66 $\pm$ 0.02 eV (see S.I. for additional sites and sample). These values are consistent with the values recently reported in the literature on similar PbSe QD solids.[20]. Now, we compare this value with theoretical results. The band structure and density of states of the PbSe superlattice has been modeled with a tight-binding theory[6, 41, 42]. The model includes broadening of the resonance peaks that describes inter-valley and electron-phonon couplings as main contributions (see below). The system is built with spherical nanocrystals and two sizes have been considered $D_1 = 5.51$ nm and $D_2 = 6.12$ nm. These sizes are chosen with respect to an interger number of the lattice constant of PbSe, D_1 corresponds to $n = 9$ unit cells, and D_2 to $n = 10$ unit cells. The nanocrystals are connected via crystalline cylinders of diameters $d_1 = 2.76$ nm and
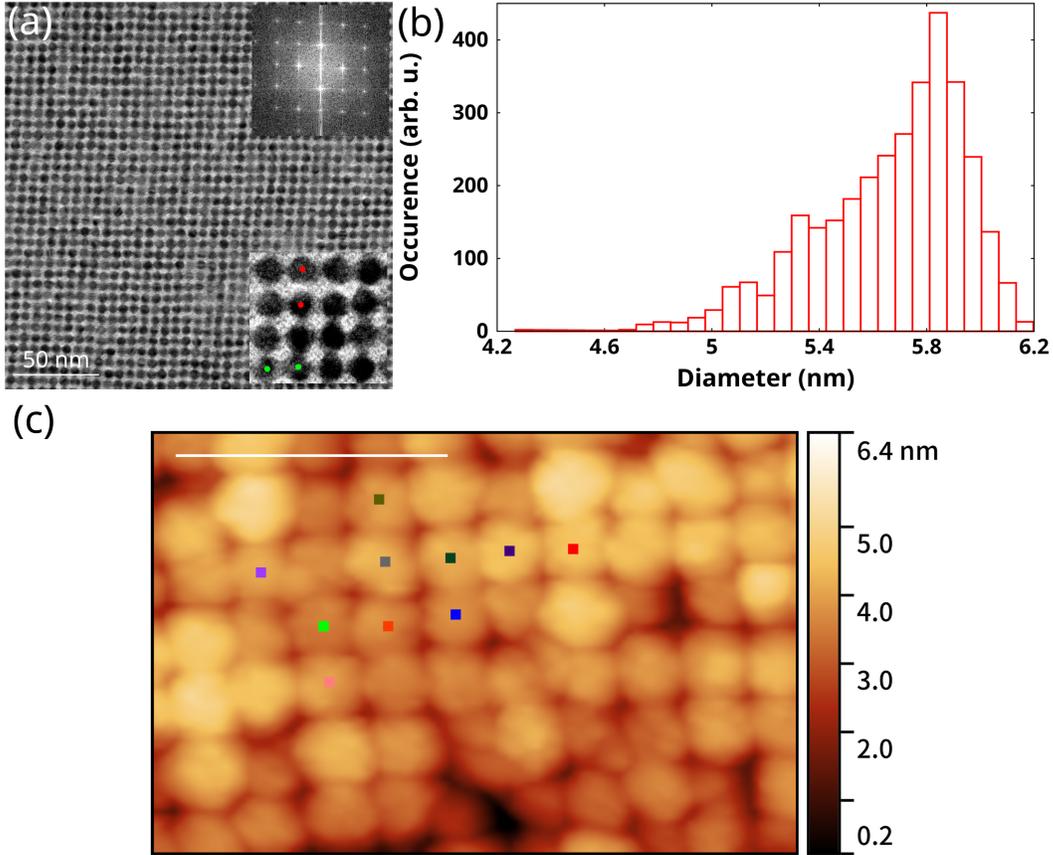
Figure 1. (a) Transmission Electron Microscope image of the square superlattice, the nanocrystals are in darker contrast while the voids in the lattice are in bright. Insets: top right, fast Fourier transform of the image presenting a center-to-center distance of 6.4 nm ± 0.2 nm and bottom right, zoom of the TEM image displaying non-existent necking (bridge between the two nanocrystals labeled with red dots) and strong necking (bridge between the two nanocrystals labeled with green dots). (b) Nanocrystal size distribution measured over 1000 nanocrystals, centered around 5.8 nm. (c) STM image of a PbSe square superlattice ($I = 5$ pA, $V_{\text{gap}} = 2$ V). Spectra have been taken on the labeled nanocrystals. The scale bar represents 20 nm.

$d_2 = 3.06$ ($d_{1,2}/D_{1,2} = 0.5$, see below for details about this value) in diameter which define the coupling strength between nanocrystals[6, 41]. The tight-binding parameters for PbSe are taken from Ref. [43]. In the case of the square superlattice, tight-binding calculations give a value of 0.68 eV and 0.62 eV for the band gap, respectively for D_1 and D_2 (curve labeled TB_1 and TB_2 in the figure 2(a)). The experimental band gap values lie in between the calculated ones, consistent with the particle size distribution.

Discussion

In the following, we discuss the resonances observed in the tunneling spectra. We first remark that these resonances were robust, reproducible (over two different samples, see S.I.) and stable over more than 20 scans. The results presented in 2(a) are averaged over 20 scans to improve the signal-to-noise ratio. We observe four resonances (peaks in dI/dV) in the positive bias range, reflecting electron conduction states and two resonances in the negative bias related to the valence hole states. The first peak (labeled e_1 in the figures 2(a) and 2(b)) of the conduction band, located at -0.05 eV $\pm$ 0.02 eV reflects the coupling of nanocrystal states with $1S_e$ envelope wavefunction. It is situated below the Fermi level (zero bias), suggesting a heavily doped structure. The composition of the PbSe nanocrystal building blocks is not stoichiometric[31]. There is a variable excess of Pb atoms at the surface of the nanocrystals (due to the $Pb(OA)_2$ that binds to dangling Se^{2-} at the surface) which causes an unintentional n-doping of the structure[28, 44, 45]. The second peak (e_2) situated at 0.11 eV $\pm$ 0.01 eV in the conduction band is attributed to the $1P_e$ envelope.

In the valence band, the first peak (h_1), situated at -0.70 eV $\pm$ 0.01 eV is the $1S_h$. The second peak h_2 at -0.78 eV $\pm$ 0.01 eV is attributed the $1P_h$ group. The relative close values of the $1S_h$ and $1P_h$ are due to the different valence band maxima (located at the L, Σ and near the K point of the Brillouin zone) of the PbSe band structure for QDs[46].

By taking into account an energy shift of -0.51 eV of the calculated electronic levels due to the doping, the conduction resonances and valence resonances agree well with the atomistic tight-binding calculations for a square PbSe lattice, see figure 2(a). Figure 2(b) presents the band structure calculations based on a building block size of 6.12 nm and a coupling $d/D = 0.5$. The different band folds are clearly visible and labeled as presented above.

Optical absorption spectroscopy has been conducted in parallel to the STS experiments. Figure 2(c) shows the absorption spectra for the dispersed nanocrystals in solution (before attachment) and for the square superlattice. The first excitonic peak for both curves represents the $1S_h$ to $1S_e$ transition and is a direct measurement of the band gap[46]. Superlattice formation results in a lowering of the band gap from 0.71 eV to 0.68 eV, which agrees well with the band gap measured by STS and the tight-binding calculations. With the observed reduction of the QD size, the measured band gap should have increased. However, the decrease of the band gap upon supercrystal synthesis suggests that there is a formation of a 2D system with creation of crystalline necks between nanocrystals of the superlattice. The broadening of the first optical transition results from this quantum mechanical coupling, but may also reflect local disorder (due to variability in nanocrystal sizes and attachment) and effects of light scattering. The later is due to the high dielectric constant of PbSe, and slight disorder in the lattice on a scale of the order of a quarter wavelength (which is still many unit cells of the square superlattice).
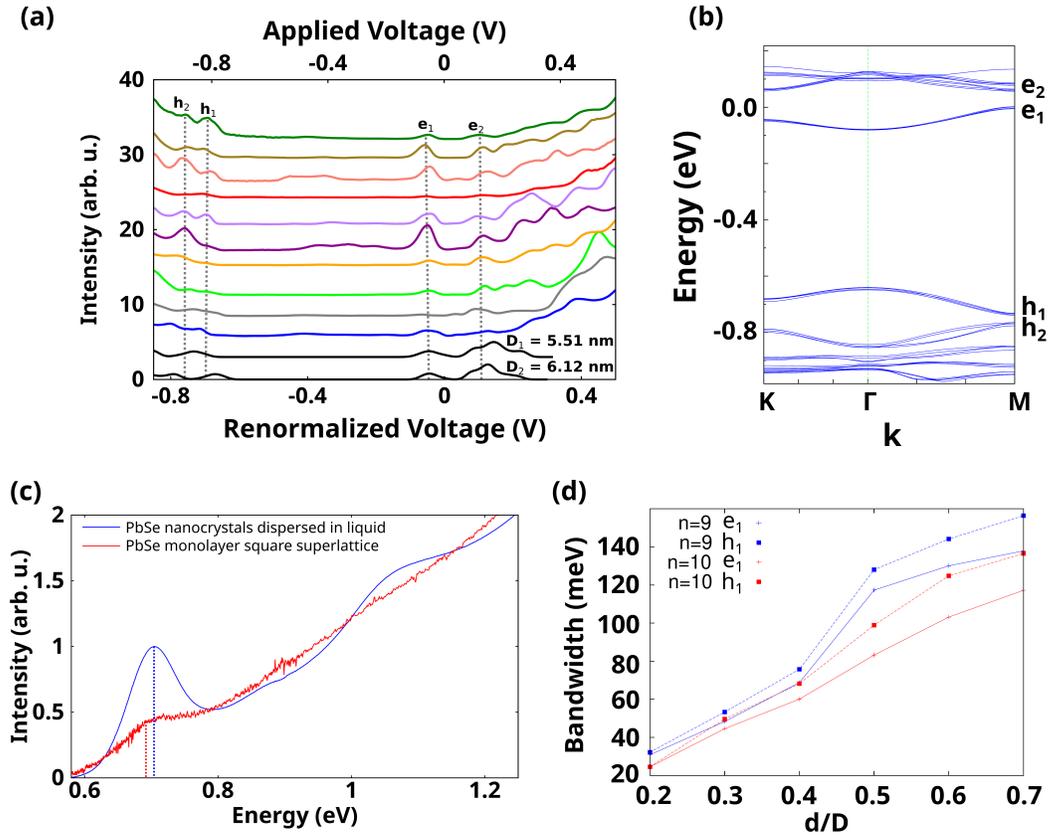
Figure 2. (a) Tunneling spectroscopy ($I = 500$ pA) on ten different nanocrystals in the superlattice (color codes correspond to colored squares in figure 1). A lever-arm $\eta = 0.85$ has been taken into account to define the renormalized voltage. The projected density of states from the tight-binding calculation is shown at the bottom. (b) Band structure of the PbSe square superlattice calculated with a unit cell composed of one nanocrystal of $D = 6.12$ nm and projected along the direction K-Γ-M. (c) Absorption spectra of dispersed PbSe nanocrystals in solution and of a monolayer of PbSe superlattice. The red shift indicates a coupling between the nanocrystals. The dotted line shows the position of the first level transition ($1S_h$ to $1S_e$) in both measurements, reflecting the value of the band gap. For the dispersed nanocrystals, the value is 0.71 eV and for the superlattice, the band gap is 0.68 eV. Amplitude of red spectrum has been renormalized with respect to the blue spectrum to better show the difference in peaks positions. (d) Bandwidth of the s-type bands in conduction (e_1) and valence (h_1) bands for the two considered nanocrystal sizes D_1 ($n = 9$) and D_2 ($n = 10$).

We now turn to the width of the observed STS peaks, as these provide information about the quantum mechanical coupling (hopping parameter in a tight-binding point of view) between nanocrystals[41, 42, 47]. A strong quantum mechanical coupling induces an important wavefunction overlap between nanocrystals and therefore large STS resonances. Inversely, a weak coupling give narrow resonance widths. The average full-widths of the e_1 and h_1 resonances of the superlattices are 103 meV $\pm$ 5 meV (e_1) and 110 $\pm$ 20 meV respectively, see figures 3(a) and (b). From our atomistic tight-binding calculations, it is possible to extract the full-width dispersion of the different band folds by taking the difference in energy between the highest and lowest energy bands in each fold. The result is presented in figure 2(d). As expected, the band width increases with increasing d for both the e_1 and h_1 bands, for both nanocrystal sizes considered. The experimental values (see figure 3) are very close to our tight-binding calculations for $d/D = 0.5$. In addition to an atomistic tight-binding model, the electronic structure of the superlattice can also be modeled using a tight-binding approach using the S_e and S_h envelope states of the QDs themselves. To first order, the dispersion of the e_1 and h_1 bands is proportional to $2t_1$ and $2t_2$, where t_1 and t_2 describe the effective coupling strength between the nanocrystals due to S_e (e_1) and S_h (h_1) states. Hence, we find an upper limit for the electronic coupling between nanocrystals of 60 meV and 65 meV for the e_1 and h_1 states, respectively.

Fluctuations in the width of the peaks can arise due to differences in the necking (and therefore coupling strength, see figures 1(a) and 3). We observe significant fluctuations in the width of the resonances (and couplings) for both electron and hole states. This is consistent with the connectivity of nanocrystals observed in TEM. In addition, the magnitude of the intervalley coupling, and therefore the peak width, depends on QDs size[48]. Coupling of the tunnelling electrons with acoustic or optical phonons can increase the peak width. At 5 K, the temperature of the measurement, extra phonon resonances are expected at the high-energy side of the principal peak. This has been observed in the case of CdSe nanocrystals[49]. However asymmetric peak broadening is not observed in the present case, excluding electron-phonon coupling as a main physical origin of broadening. It is of interest to compare the present results with those obtained on individual QDs and for a lattice with close-packed PbSe NC ordering that has been strongly annealed[50]. In the former, the width of the resonances are smaller (around 75 $\pm$ 15 meV) than the values found in our measurements[48]. In the latter, the variations in the widths of the resonances and the band gaps were much more pronounced than observed here. In the present case, the band structure of the square superlattices and the width of the resonances are much more uniform, with a moderate electronic coupling between the NCs.

The TEM and STM images show that there is a distribution in the size of the building blocks and the width of the crystalline necks between the nanocrystals (see figure 1). A certain variation in the energy of the on-site s- and p-states should therefore be expected. However, our results indicate that the variations of the on-site energies
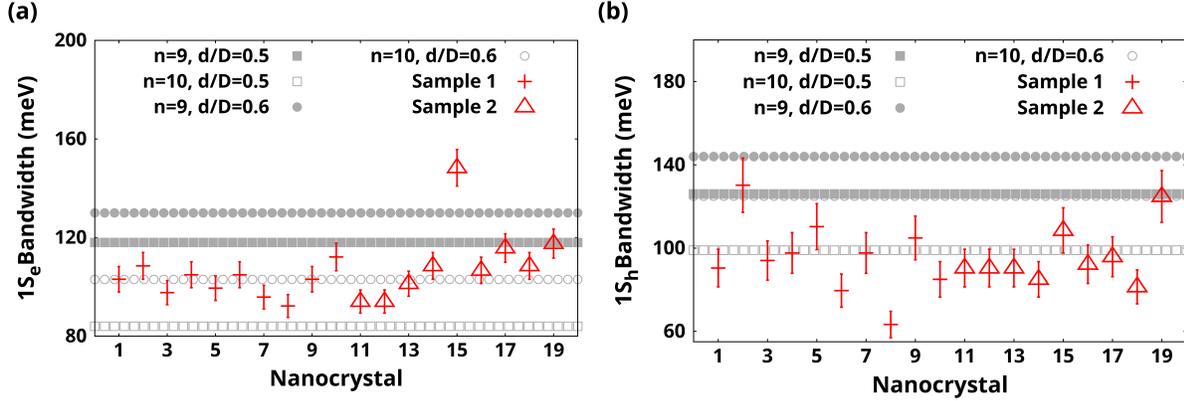
Figure 3. (a) Bandwidths of the $1S_e$ bands in the conduction band for two different samples (crosses for the sample 1, triangles for sample 2, see S.I. for more details) compared to calculated dispersions for superlattices composed of nanocrystals with diameter of $D_1 = 5.5$ nm (filled symbols) and $D_2 = 6.1$ nm (open symbols) and for each, two necking sizes $d/D = 0.5$ (circles) and $d/D = 0.6$ (squares). (b) Same comparison for the valence band including the bandwidths of the $1S_h$ bands.

are small (see S.I). Hence, we attribute the fluctuations in peak width to differences in the width and crystallinity of the necks between individual QDs.

Careful inspection of the dI/dV spectra in the gap region reveals that there may be some in-gap states present in the array. It is unlikely to be noise because the amplitude of those peaks saturates with high current set-point (see S.I.). The presence of those peaks are attributed to trap states. Such trap states, could come from the detachment of ligands from certain selenium and lead atoms at the surface of the nanocrystals as seen for other II-VI nanocrystals[51]. The saturation is explained by state filling for these localized states, while tunneling via the delocalized band states remains in the shell-tunneling regime[52]. Those states are highly localized states at the surface of the nanocrystals, causing a drastic reduction of the probability for electrons in those states to tunnel out of the nanocrystal. The shell-filling regime is often associated with double peaks due to the additional energy needed to inject another electron in those already occupied states. Here, no double peak is visible because of the large dielectric constant of the PbSe resulting in Coulomb energy of only a few meV.

Superlattices of semiconductors nanocrystals are considered to become a class of novel electronic materials once the electronic coupling between the NCs is strong enough, and once the strucral disorder is sufficiently small. There is an ongoing discussion on the nature of the carrier transport and convincing evidence for band-like transport has not been presented yet.

In order to improve the electronic coupling and lower the disorder. It is imperative to use a nanocrystal solution with the smallest possible distributions in size and shape. The shape of nanocrystals can be modified by the ligand density, leading to smoother nanocrystalline facets[53]. The forces that keep the nanocrystals in the assembly

plane can be tweaked by having higher solvent-air surface tension[54]. One of the sources of non-uniform necking is the angular variation between [100] facets[18, 22, 55] and, assembly and post-treatment techniques aim to improve the regularity of such superlattices.

Conclusion

In conclusion, we have measured the local density of states of a square superlattice made of PbSe semiconductor nanocrystals. The STM image of the annealed sample revealed a clean surface where it was possible to acquire reproducible scanning tunneling spectra. Those spectra showed a band gap of 0.66 eV in agreement with tight-binding calculations and optical spectroscopy measurements. The peak widths for the first energy levels were close to our atomistic tight-binding calculations for coupling of $d/D = 0.5$. By comparing the experimentally determined bandwidths with tight-binding simulations, we find an upper limit of 65 meV for the coupling (hopping term) between the nanocrystals in the superlattice. There are significant fluctuations in the observed band-widths, consistent with large differences in the necking between QDs as observed in TEM images. Band-like electronic coupling will require more homogeneous couplings and ideally stronger crystalline neckings between the nanocrystals.

Acknowledgement

References

[1] von Klitzing K 1986 *Rev. Mod. Phys.* **58**(3) 519–531
[2] Bernevig B A, Hughes T L and Zhang S C 2006 *Science* **314** 1757–1761
[3] König M, Wiedmann S, Brüne C, Roth A, Buhmann H, Molenkamp L W, Qi X L and Zhang S C 2007 *Science* **318** 766–770
[4] Park C H, Yang L, Son Y W, Cohen M L and Louie S G 2008 *Nat. Phys.* **4** 213–217
[5] Park C H and Louie S G 2009 *Nano Lett.* **9** 1793–1797
[6] Kalesaki E, Delerue C, Morais Smith C, Beugeling W, Allan G and Vanmaekelbergh D 2014 *Phys. Rev. X* **4**(1) 011010
[7] Gomes K K, Mar W, Ko W, Guinea F and Manoharan H C 2012 *Nature* **483** 306
[8] Slot M R, Gardenier T S, Jacobse P H, van Miert G C P, Kempkes S N, Zevenhuizen S, Smith C M, Vanmaekelbergh D and Swart I 2017 *Nat. Phys.* **13** 672
[9] Slot M R, Kempkes S N, Knol E J, van Weerdenburg W M J, van den Broeke J J, Wegner D, Vanmaekelbergh D, Khajetoorians A A, Morais Smith C and Swart I 2019 *Phys. Rev. X* **9** 011009
[10] Drost R, Ojanen T, Harju A and Liljeroth P 2017 *Nat. Phys.* **13** 668–671
[11] Wang S, Scarabelli D, Du L, Kuznetsova Y Y, Pfeiffer L N, West K W, Gardner G C, Manfra M J, Pellegrini V, Wind S J and Pinczuk A 2018 *Nat. Nano.* **13** 29–33
[12] Nádvorník L, Orlita M, Goncharuk N A, Smrčka L, Novák V, Jurka V, Hruška K, Výborný Z, Wasilewski Z R, Potemski M and Výborný K 2012 *New J. Phys.* **14** 053002

[13] Post L C, Xu T, Vergel N A F, Tadjine A, Lambert Y, Vaurette F, Yarekha D, Desplanque L, Stiévenard D, Wallart X, Grandidier B, Delerue C and Vanmaekelbergh D 2019 *Nanotech.* **30** 155301

[14] Franchina Vergel N A, Post L C, Sciacca D, Berthe M, Vaurette F, Lambert Y, Yarekha D, Troadec D, Coinon C, Fleury G, Patriarche G, Xu T, Desplanque L, Wallart X, Vanmaekelbergh D, Delerue C and Grandidier B 2021 *Nano Lett.* **21** 680–685

[15] Boneschanscher M P, Evers W H, Geuchies J J, Altantzis T, Goris B, Rabouw F T, van Rossum S A P, van der Zant H S J, Siebbeles L D A, Van Tendeloo G, Swart I, Hilhorst J, Petukhov A V, Bals S and Vanmaekelbergh D 2014 *Science* **344** 1377–1380

[16] Liljeroth P, Overgaag K, Urbieta A, Grandidier B, Hickey S G and Vanmaekelbergh D 2006 *Phys. Rev. Lett.* **97**(9) 096803

[17] Overgaag K, Liljeroth P, Grandidier B and Vanmaekelbergh D 2008 *ACS Nano* **2** 600–606

[18] Peters J L, Altantzis T, Lobato I, Jazi M A, van Overbeek C, Bals S, Vanmaekelbergh D and Sinai S B 2018 *Chem. Mater.* **30** 4831–4837

[19] Whitham K, Yang J, Savitzky B H, Kourkoutis L F, Wise F and Hanrath T 2016 *Nat. Mater.* **15** 557

[20] Ueda S T, Kwak I, Abelson A, Wolf S, Qian C, Law M and Kummel A C 2020 *Appl. Surf. Sci.* **513** 145812

[21] Maier A, Lapkin D, Mukharamova N, Frech P, Assalauova D, Ignatenko A, Khubbutdinov R, Lazarev S, Sprung M, Laible F, Löffler R, Previdi N, Bräuer A, Günkel T, Fleischer M, Schreiber F, Vartanyants I A and Scheele M 2020 *Adv. Mater.* **32** 2002254

[22] Walravens W, Solano E, Geenen F, Dendooven J, Gorobtsov O, Tadjine A, Mahmoud N, Ding P P, Ruff J P C, Singer A, Roelkens G, Delerue C, Detavernier C and Hens Z 2019 *ACS Nano* **13** 12774–12786

[23] Smeaton M A, El Baggari I, Balazs D M, Hanrath T and Kourkoutis L F 2021 *ACS Nano* **15** 719–726

[24] Chu X, Heidari H, Abelson A, Unruh D, Hansen C, Qian C, Zimanyi G, Law M and Moulé A J 2020 *J. Mater. Chem. A* **8**(35) 18254–18265

[25] Ondry J C, Philbin J P, Lostica M, Rabani E and Alivisatos A P 2021 *ACS Nano* **15** 2251–2262

[26] Chen I Y, Cimada daSilva J, Balazs D M, Smeaton M A, Kourkoutis L F, Hanrath T and Clancy P 2020 *ACS Nano* **14** 11431–11441

[27] Swart I, Liljeroth P and Vanmaekelbergh D 2016 *Chem. Rev.* **116** 11181–11219

[28] Evers W H, Schins J M, Aerts M, Kulkarni A, Capiod P, Berthe M, Grandidier B, Delerue C, van der Zant H S J, van Overbeek C, Peters J L, Vanmaekelbergh D and Siebbeles L D A 2015 *Nat. Comm.* **6** 8195

[29] Alimoradi Jazi M, Kulkarni A, Sinai S B, Peters J L, Geschiere E, Failla M, Delerue C, Houtepen A J, Siebbeles L D A and Vanmaekelbergh D 2019 *J. Phy. Chem. C* **123** 14058–14066

[30] Steckel J S, Yen B K H, Oertel D C and Bawendi M G 2006 *J. Am. Chem. Soc.* **128** 13032–13033

[31] Moreels I, Lambert K, De Muynck D, Vanhaecke F, Poelman D, Martins J C, Allan G and Hens Z 2007 *Chem. Mater.* **19** 6101–6106

[32] Evers W H, Goris B, Bals S, Casavola M, de Graaf J, van Roij R, Dijkstra M and Vanmaekelbergh D 2013 *Nano Lett.* **13** 2317–2323

[33] van Overbeek C, Peters J L, van Rossum S A P, Smits M, van Huis M A and Vanmaekelbergh D 2018 *J. Phys. Chem. C* **122** 12464–12473

[34] Geuchies J J, van Overbeek C, Evers W H, Goris B, de Backer A, Gantapara A P, Rabouw F T, Hilhorst J, Peters J L, Konovalov O, Petukhov A V, Dijkstra M, Siebbeles L D A, van Aert S, Bals S and Vanmaekelbergh D 2016 *Nat. Mater.* **15** 1248

[35] Peters J L, van der Bok J C, Hofmann J P and Vanmaekelbergh D 2019 *Chem. Mater.* **31** 5808–5815

[36] Li D, Nielsen M H, Lee J R I, Frandsen C, Banfield J F and De Yoreo J J 2012 *Science* **336** 1014–1018

[37] Castellanos-Gomez A, Rubio-Bollinger G, Garnica M, Barja S, de Parga A L V, Miranda R and Agraït N 2012 *Ultramicroscopy* **122** 1–5

[38] Tewari S, Bastiaans K M, Allan M P and van Ruitenbeek J M 2017 *Beilstein J. Nanotechnol.* **8** 2389–2395

[39] Franceschetti A, Williamson A and Zunger A 2000 *J. Phys. Chem. B* **104** 3398–3401

[40] Niquet Y M, Delerue C, Allan G and Lannoo M 2002 *Phys. Rev. B* **65** 165334

[41] Kalesaki E, Evers W H, Allan G, Vanmaekelbergh D and Delerue C 2013 *Phys. Rev. B* **88**(11) 115431

[42] Delerue C 2014 *Phys. Chem. Chem. Phys.* **16**(47) 25734–25740

[43] Allan G and Delerue C 2004 *Phys. Rev. B* **70**(24) 245321

[44] Gai Y, Peng H and Li J 2009 *J. Phys. Chem. C* **113** 21506–21511

[45] Oh S J, Berry N E, Choi J H, Gaulding E A, Paik T, Hong S H, Murray C B and Kagan C R 2013 *ACS Nano* **7** 2413–2421

[46] An J M, Franceschetti A, Dudiy S V and Zunger A 2006 *Nano Lett.* **6** 2728–2735

[47] Delerue C and Vanmaekelbergh D 2015 *2D Mater.* **2** 034008

[48] Overgaag K, Vanmaekelbergh D, Liljeroth P, Mahieu G, Grandidier B, Delerue C and Allan G 2009 *J. Chem. Phys.* **131** 224510

[49] Sun Z, Swart I, Delerue C, Vanmaekelbergh D and Liljeroth P 2009 *Phys. Rev. Lett.* **102**(19) 196401

[50] Liljeroth P, van Emmichoven P A Z, Hickey S G, Weller H, Grandidier B, Allan G and Vanmaekelbergh D 2005 *Phys. Rev. Lett.* **95**(8) 086801

[51] Houtepen A J, Hens Z, Owen J S and Infante I 2017 *Chem. Mater.* **29** 752–761

[52] Berthe M, Stiufiuc R, Grandidier B, Deresmes D, Delerue C and Stiévenard D 2008 *Science* **319** 436–438

[53] Peters J L, van den Bos K H W, Van Aert S, Goris B, Bals S and Vanmaekelbergh D 2017 *Chem. Mater.* **29** 4122–4128

[54] Soligno G and Vanmaekelbergh D 2019 *Phys. Rev. X* **9** 021015

[55] McCray A R C, Savitzky B H, Whitham K, Hanrath T and Kourkoutis L F 2019 *ACS Nano* **13** 11460–11468